Electronic Supplementary Material (ESI) for Physical Chemistry Chemical Physics.

Supporting Information for: Structural dynamics upon photoexcitation-induced charge transfer in a dicopper(I)-disulfide complex

November 20, 2017

Contents

1 Comparison of the DFT-calculated and experimental UV-Vis absorption spectra

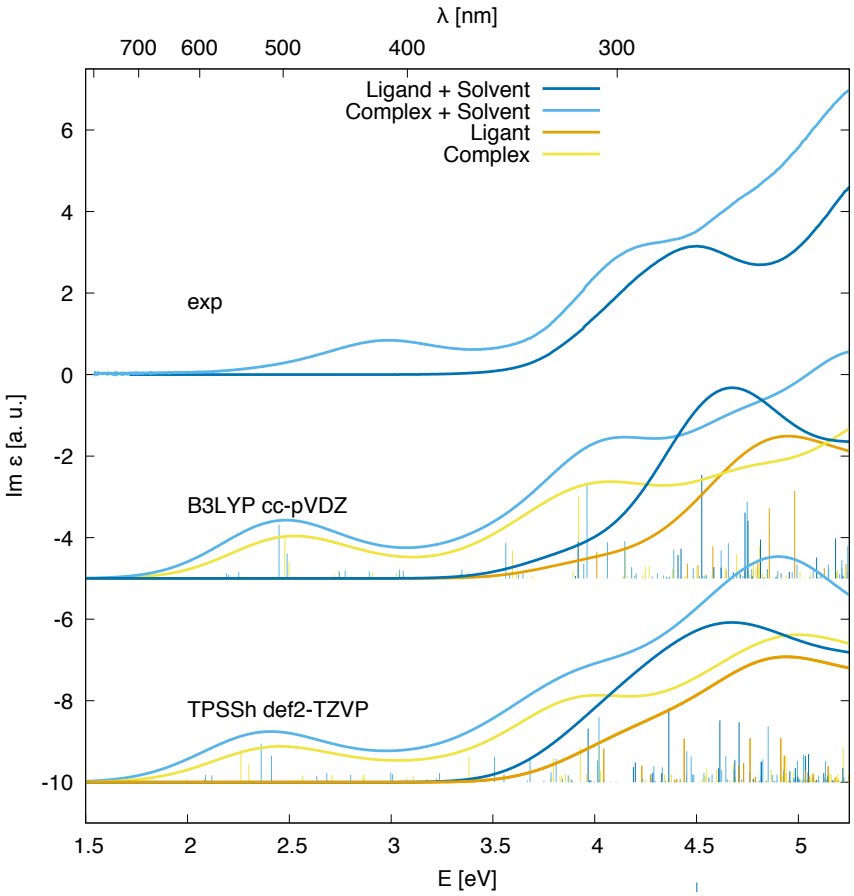

Figure S1: UV-Vis absorption spectra: experimental and calculated with DFT.

2 Ground state EXAFS: fitting in ExCurve and Artemis including structural parameters

EXAFS spectra of solid $[Cu_2(NguaS{-}SNgua)_2]OTf_2$ at the Cu K-edge and of 10 mM solution of $[Cu_2(NguaS{-}SNgua)_2](OTf)_2$ in acetonitrile look almost identical, as shown in Fig.S2, which confirms that the complex is intact at this concentration in the acetonitrile solution and there are no or only negligible influences of coordinating acetonitrile molecules visible.

In the main text of the paper the EXAFS spectrum of solid $[Cu_2(NguaS{-}SNgua)_2](OTf)_2$ is fitted using Artemis and varying only non-structural parameters, which is necessary for the subsequent TR-EXAFS analysis. The used scattering paths and the fitting parameters are gathered in Table S1. The following parameters were used as the input to feff8.5L for both GS and future ES $\chi(k)$ calculation: RMAX 5.0; NLEG 4; FOLP 0 1.1; AFOLP; SCF 5 1. FOLP for the central atom was set to 1.1 because with the standard FOLP = 1.15 the calculation failed.

In order to check the reliability of the EXAFS fit with non-structural parameters, fitting of the data including the structural parameters was performed on both solid $Cu_2(NSSN)_2$ and its acetonitrile solution. Data reduction and fitting was performed independently with ExCurve [1] and with Athena and Artemis [9] software packages. The comparative fitting results are presented in the Table S1 (Excurve: solid OTf^- and 10 mM acetonitrile solution; Artemis: solid

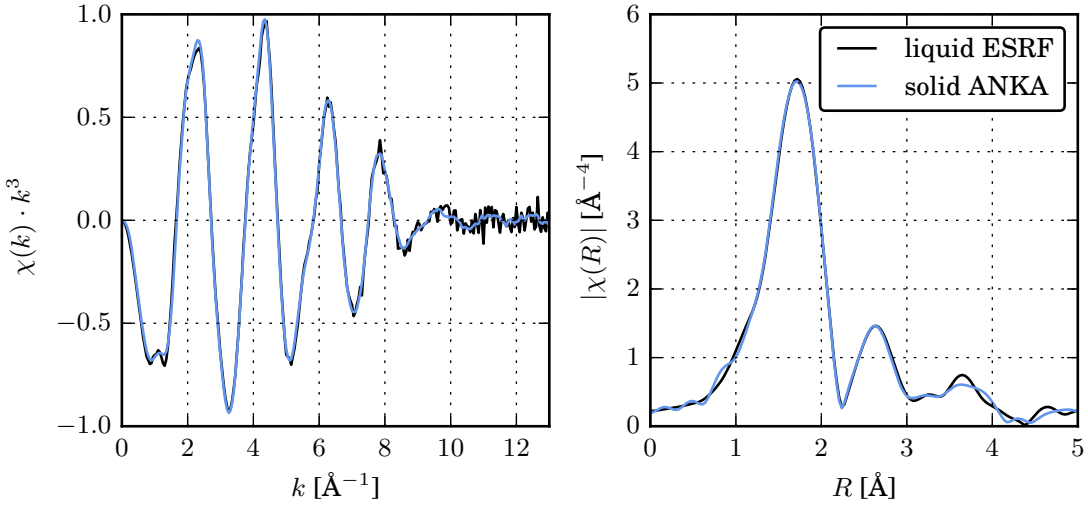

Figure S2: Comparison of $\chi(k)$ and the corresponding Fourier transforms between EXAFS spectra of solid $[Cu_2(NSSN)_2](OTf)_2$ and its 10 mM solution in acetonitrile.

Table S1: List of scattering paths included in the non-structural fit and the fitting results. $S_0^2 = 1$, $E_0 = -0.2 \pm 0.4$ eV. The atoms are marked as in Fig.S3. N_{ind} = 25, N_{par} = 8.

Scattering path	σ^2 [Å^2]	fitting parameter
Cu-$N_{(d)}$	0.0079±0.0008	sig1
Cu-$S_{(g)}$	0.0109±0.0006	sig2
Cu-$C_{(c,e,f)}$	0.0087±0.0016	sig3
Cu-$C_{(e)}$-$C_{(f)}$	0.0087±0.0016	sig3
Cu-$N_{(d)}$ -$C_{(e,c)}$	0.007±0.004	sig_ms
Cu-$N_{(d)}$ -$C_{(e,c)}$-$N_{(d)}$	0.016±0.004	sig1·2
Cu-$N_{(b)}$,Cu-$C_{(a)}$	0.030±0.016	sig4
Cu-$N_{(d)}$ -$C_{(f)}$	0.0083±0.0009	sig1/2+sig3/2
Cu-$N_{(d)}$ -$N_{(b)}$	0.019±0.007	sig1/2+sig4/2
Cu-$S_{(g)}$ -$C_{(f)}$	0.0098±0.0008	sig2/2+sig3/2
Cu-$S_{(h)}$	0.017±0.013	sig5
Cu-Cu	0.021± 0.013	sig6

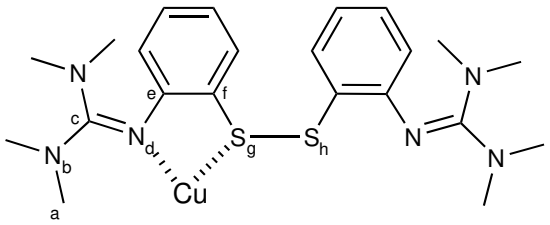

Figure S3: Atoms indicated in the EXAFS fitting results (Table S1).

Table S2: Comparative results of EXAFS fitting performed in Artemis and ExCurve. For details see text.

		Solid, ExCurve	Solution, ExCurve	Solid, Artemis	Cryst. distance [Å]
	E_0 [eV]	2.8 ± 2.2	2.9 ± 2.5	-2.6 ± 1.2	
	S_0^2	1	1.07 ± 1.15	0.9999 ± 0.0002 (restrained by 1)	
N	N	1.9±1.2	1.7±2.2	2	2
	R [Å]	2.00±0.03	1.99±0.04	2.017±0.015	2.021±0.010
	σ^2 [a]	0.021±0.007	0.021±0.009	0.009 ±0.001	
S	N	2.3±1.2	2.4±3.1	2	2
	R [Å]	2.26±0.02	2.25±0.02	2.276±0.009	2.288±0.011
	σ^2	0.024±0.007	0.021±0.009	0.0109±0.0008	
C	N	3.4±1.4	2.8±3.8	6	6
	R [Å]	2.90±0.02	2.90±0.02	2.87,2.95,3.00±0.02	2.898-3.067
	σ^2	0.021±0.009	0.018±0.009	0.012±0.002	av. = 2.964
S	N	1.7±0.8	1.7±2.7	2	2
	R [Å]	3.51±0.03	3.50±0.03	3.57±0.03	3.400-3.659
	σ^2	0.025±0.011	0.025±0.013	0.016±0.004	av. = 3.530
Cu	N	1.0±0.8	1	1	1
	R [Å]	3.96±0.03	3.95±0.04	4.02±0.03	3.941
	σ^2	0.025±0.011	0.025±0.015	0.013±0.004	

[a] σ^2 values from ExCurve should be divided by 2 to be compared with Artemis

OTf^-).

ExCurve. Scattering atoms were added shell by shell, and their number, distance to the absorber and σ^2 were fitted. Five shells were included: N, S, C, S, Cu. Since there was no 3D model, only single scattering paths were considered. C_a and N_b (see Fig.S3) were not considered in the fit, because they could not be fitted with reasonable parameters. The results are presented in Fig.S4 and S5.

Artemis. Relaxed D_2 3D model based on the DFT calculation of the ground state structure was used. The same shells were included into the fit as in ExCurve (N,S,C,S,Cu). Using 3D model allowed us to additionally include multiple scattering paths. The results are presented in Fig.S6.

The fitting parameters for all analysis sets are gathered in Table S2. Both software packages yield similar results that confirm the crystallographic structure. The distances to the coordinating atoms (N and S) match within errorbars for two software packages; for further shells there are some discrepancies due to the contribution of multiple scattering paths taken into account in Artemis fit.

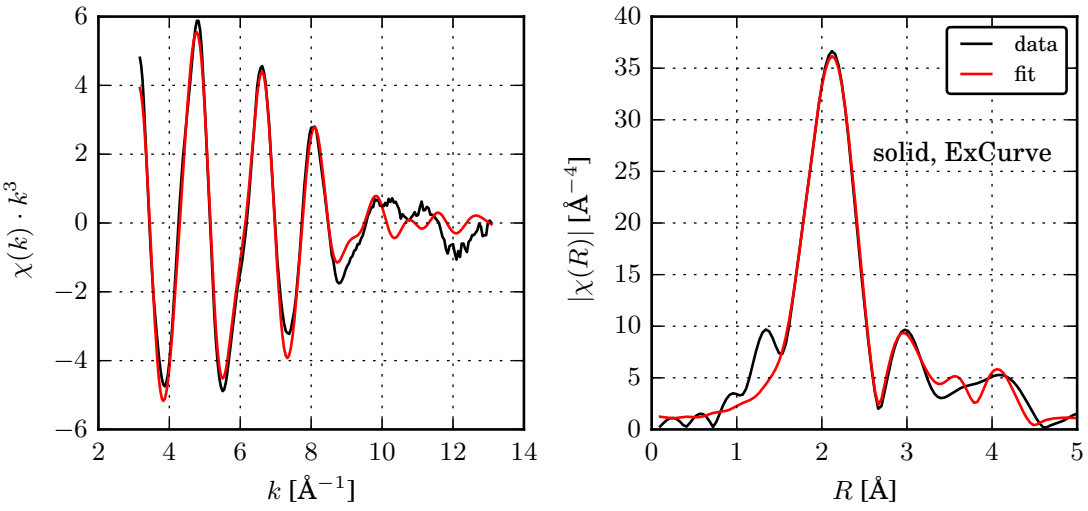

Figure S4: Fit of EXAFS of solid state $Cu_2(NSSN)_2(OTf)_2$ performed with ExCurve. N, S, C, S, Cu shells were included; number of atoms, distances to shells and σ^2 were fitted.

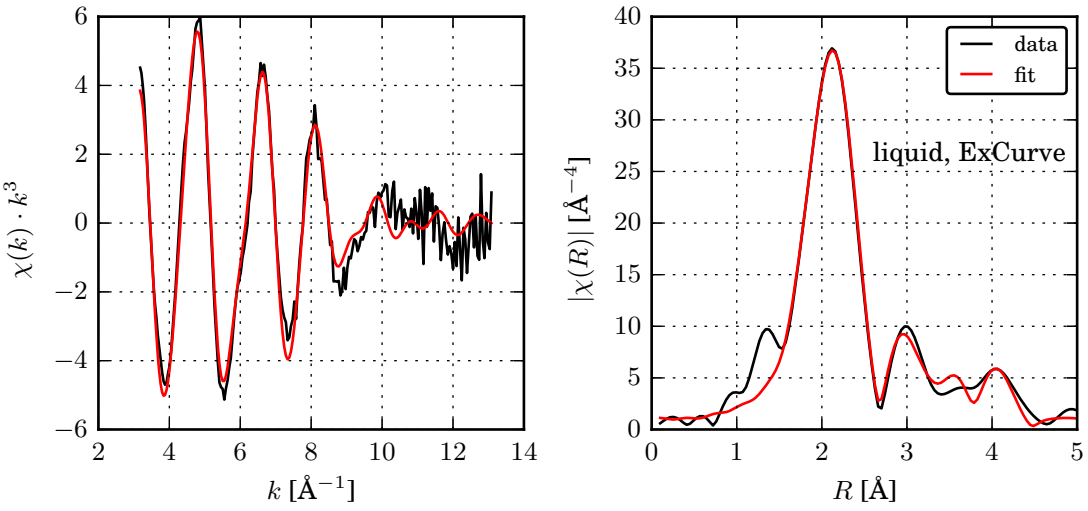

Figure S5: Fit of EXAFS of 10 mM acetonitrile solution of $Cu_2(NSSN)_2(OTf)_2$ performed with ExCurve. N, S, C, S, Cu shells were included; number of atoms, distances to shells and σ^2 were fitted.

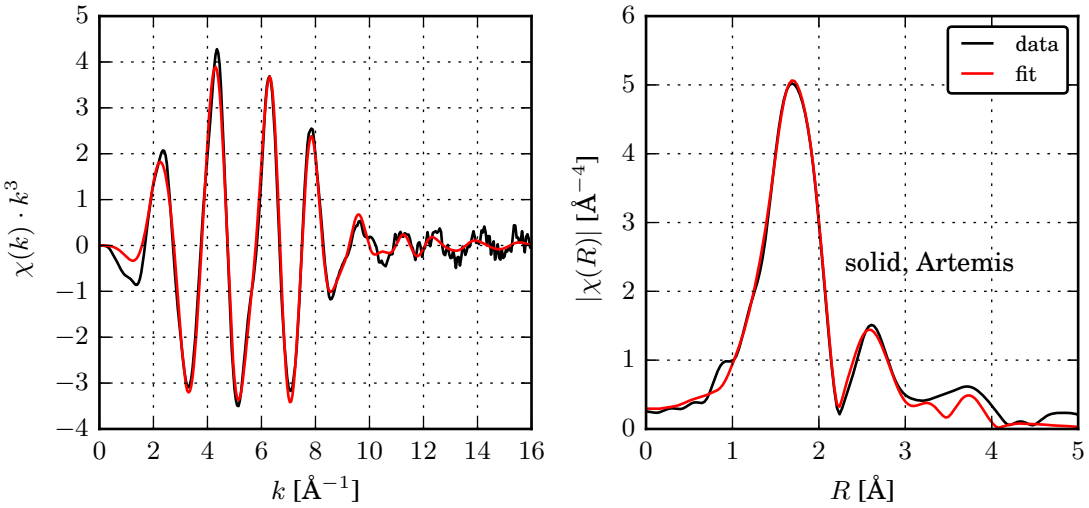

Figure S6: Fit of EXAFS of solid state $Cu_2(NSSN)_2(OTf)_2$ performed with Artemis. N, S, C, S, Cu shells were included; distances to shells and σ^2 were fitted. The number of atoms was taken from the crystallographic data and was not refined.

3 Estimation of the excited state fraction in the TR-XAS experiment

The laser-pumped spectrum has contributions of both ground and excited state spectra. In order to extract the ES spectrum, the knowledge of relative contribution of the ES spectrum (ES fraction f) is necessary. In order to estimate it, we performed the following analysis of the absorption edge.

The GS spectrum edge has two pronounced shoulders. It could be modelled as a sum of an error function and two pseudo-voigt peaks centred at 8982.36 eV (pV_1) and 8985.41 eV (pV_2) as shown in Fig. 7. In the excited state the edge is shifted to the higher energies. In the observed transient this shift manifests itself as two minima corresponding to the two edge shoulders. For a molecule containing only Cu^{+2} the shoulder at 8982.4 eV should not be present. However, since we have two copper atoms in the molecule, we assume that in the excited state the intensity of this shoulder would only drop by half instead of disappearing completely. Therefore we look for f for which the amplitude of the pV_1 in the excited state would be half of the amplitude in the ground state: $\text{amp}_{ES}(pV_1)$=0.5·$\text{amp}_{GS}(pV_1)$. In order to find this f we constructed excited state spectra assuming different values of f and fitted their lineshapes using the same model as for the GS, varying only amplitudes of the edge peaks. This way we found f=0.074 for which the condition $\text{amp}_{ES}(pV_1)$=0.5·$\text{amp}_{GS}(pV_1)$ was satisfied.

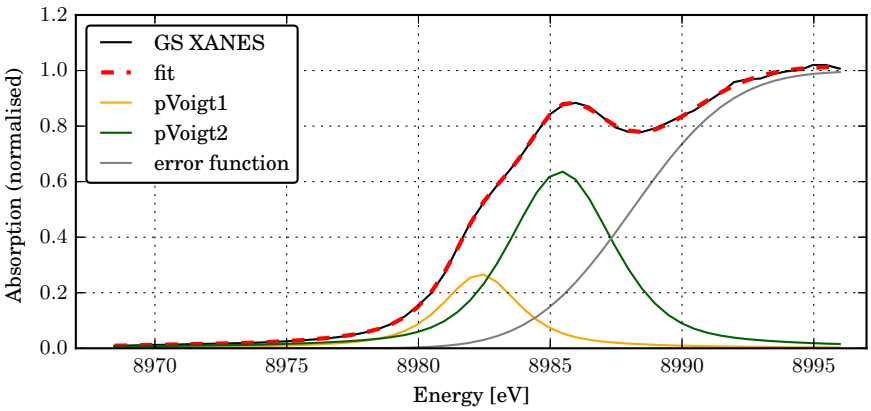

Figure S7: Modelling of the absorption edge as a sum of two pseudo-voigt functions and an error-function.

4 TR-EXAFS: data extraction

The ground and laser-pumped X-ray absorption spectra collected during the pump-probe experiment show EXAFS oscillation damping and high noise level compared to the GS spectrum obtained in a conventional EXAFS experiment at ESRF for the same solution (see Fig.S8).

As possible reasons for the oscillation damping two effects were considered: fluorescence self-absorption and the detector dead time. Fluorescence self-absorption should not have strong effect: the mass percentage of copper in a 10 mM acetonitrile solution is:

$$\frac{m_{Cu}}{m_{solution}} = \frac{c_{Cu} \cdot M_{Cu}}{c_{complex} \cdot M_{complex} + \rho_{solvent}} = 0.0075.$$

This concentration of the absorbing atom falls into the diluted sample approximation and should not show self-absorption effects in the X-ray absorption spectrum. Therefore, we assume that the saturation of the detector caused this effect. It has not been analysed further because we do not have an estimation for the count rate in the detector during the experiment. Self-absorption correction module in Athena software [9] was used in order to correct for the

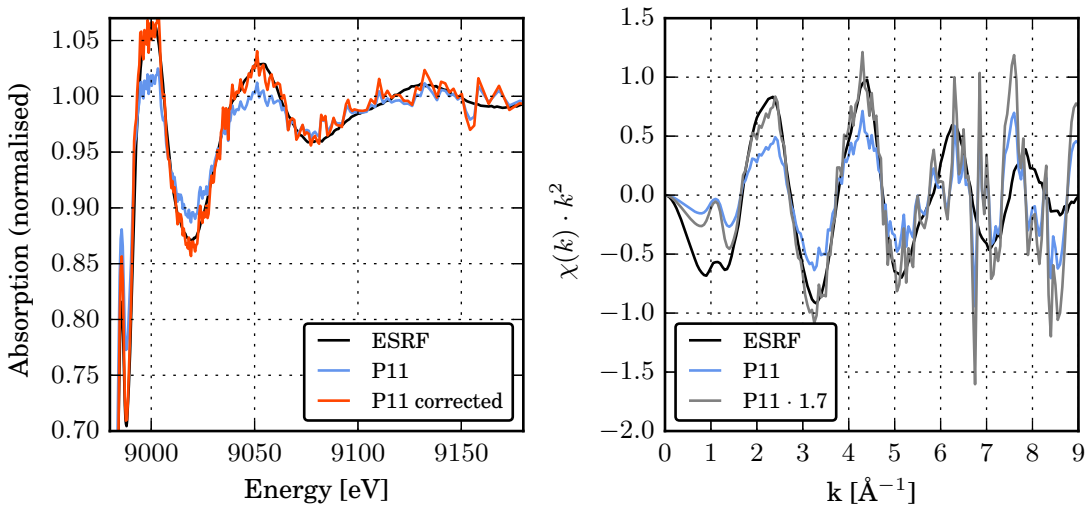

Figure S8: Comparison of X-ray absorption spectra from the pump-probe experiment (measured at P11 beamline) and a static experiment (measured in ESRF). Left: self-absorption correction was performed on the P11 data in Athena software, resulting in a good match between the two data sets. Right: EXAFS data from P11 and ESRF in k-space.

damping. The correction was performed on the data normalised by incident intensity I_0. Even though the reason for damping is different, applying this correction results in a good match between corrected data and a static spectrum as shown in Fig.S8 (left).

Despite the high noise level in the normalised GS spectrum, the transient spectrum obtained by subtracting normalised steady-state (unpumped) from normalised laser-pumped spectrum $\mathrm{Tr}_{\mathrm{norm}} = \mathrm{pumped}_{\mathrm{norm}} - \mathrm{unpumped}_{\mathrm{norm}}$ shows clear oscillations even in the regions where the steady-state and laser-pumped spectra are dominated by noise. What is more, the transient calculated by subtraction of raw signals, not normalised by I_0, $\mathrm{Tr}_{\mathrm{raw}} = \mathrm{pumped}_{\mathrm{raw}} - \mathrm{unpumped}_{\mathrm{raw}}$ demonstrates higher StN ratio than $\mathrm{Tr}_{\mathrm{norm}}$ as demonstrated in Fig.S9. Since $\mathrm{Tr}_{\mathrm{raw}}$ had higher StN ratio than $\mathrm{Tr}_{\mathrm{norm}}$, it was used as the experimental data in the further data analysis (scaled by 1.7 to compensate for damped oscillations).

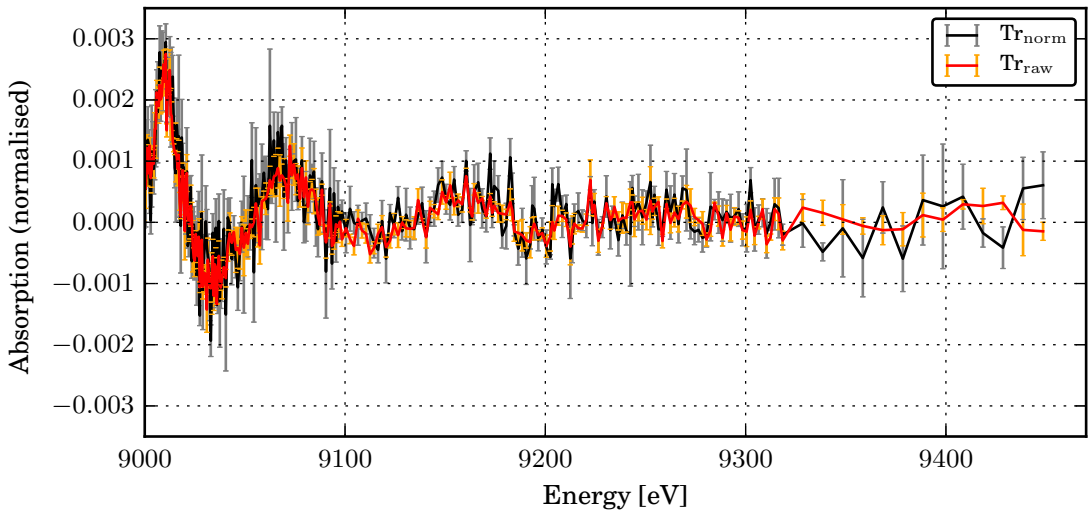

Figure S9: Comparison between $\mathrm{Tr_{raw}} = \mathrm{pumped_{raw}} - \mathrm{unpumped_{raw}}$ and $\mathrm{Tr_{norm}} = \mathrm{pumped_{norm}} - \mathrm{unpumped_{norm}}$. For the details see text. Both transients are divided dy the corresponding edge jumps.

5 TR-EXAFS: data analysis

For TR-EXAFS analysis for each parameter set (dE, f, $\mathbf{Q}$) $f \cdot \mathrm{Tr_{calc}}$ was calculated and compared to $\mathrm{Tr_{exp}}$. The agreement between the calculation and the experiment was evaluated by calculating χ^2_{red} according to the following equation:

$$\chi^2_{red} = \frac{1}{N-1} \cdot \Sigma\left(\frac{f \cdot \mathrm{Tr_{calc}}(dE, \mathbf{Q}) - \mathrm{Tr_{exp}}}{stderr}\right)^2, \tag{1}$$

where N is the number of points in the experimental spectrum, $stderr$ is standard error for experimental values. The standard deviation at each energy point j of the spectrum could be estimated as $stddev_j = \sqrt{\frac{1}{n_j - 1} \cdot \sum_{i=1}^{n_j} (x_{ij} - \overline{x_j})}$, where x_{ij} is an independent measurement at point j, n_j is the number of measurements (n_j = 3 or 6 for different parts of the spectrum). However, due to the small values of n, values of the standard deviation differed strongly from point to point, thus making some spectral points during the χ^2_{red} calculation much more (orders of magnitude) significant than others. This is not physically reasonable, because we expect approximately the same signal at all EXAFS energies. For this reason the standard deviation for each experimental data point was taken to be the same and was calculated as the mean value of standard deviations for all measurement points $stddev = \frac{1}{N} \sum_{j=1}^{N} stddev_j$. The standard error, or the standard deviation of the mean, was then calculated for each spectral point as $stderr_j = stddev / \sqrt{n_j}$.

The confidence regions for $\mathbf{Q}$, dE and f are shown in Fig.S10. Contour plots enclosing the 68.3 %, 95.5 % and 99.7 % confidence regions are plotted on the ($\mathbf{Q}$, dE) space for different values of f. The overlap of these confidence regions for all values of f builds the final confidence region. The error bars for the values of $\mathbf{Q}$, dE and f in the main text are given as values covering 68.3 % confidence interval.

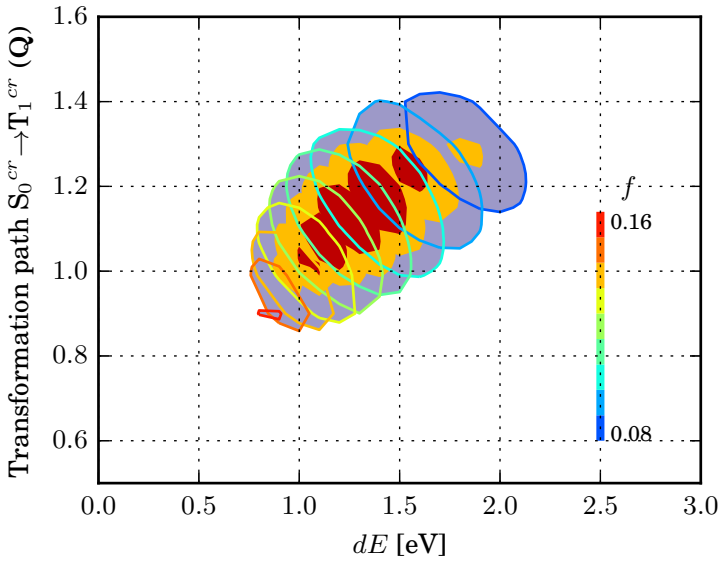

Figure S10: Confidence regions of the transient EXAFS fit on the field of (**Q**, dE) parameters. Red areas show 68.3 %, yellow areas – 95.5 %, and transparent violet – 99.7 % confidence regions. For the 99.7 % region contour lines corresponding to different excited state fractions are shown.

Table S3: TR-EXAFS analysis: best fit results for structures along $S_0^{cr} \rightarrow T_1^{cr}$ transformation path (**Q**).

Q	f	dE [eV]	χ^2_{red}
0.5	0.185	0.5	1.93
0.6	0.190	1.0	1.64
0.7	0.17	1.0	1.59
0.8	0.155	1.0	1.54
0.9	0.145	1.0	1.51
1.0	0.125	1.1	1.48
1.1	0.115	1.2	1.47
1.2	0.10	1.4	1.47
1.3	0.09	1.5	1.48
1.4	0.08	1.7	1.52
1.5	0.07	2.	1.56
1.6	0.065	2.1	1.62

6 Estimation of the excited state fraction in the different pump-probe experiments in this work

In general, one way to estimate the excited state fraction in the laser-illuminated volume is to calculate the fraction of molecules that absorbed incoming laser photons. This value is not exactly the excited state fraction observed in the experiment due to some reasons. Namely, in this calculation there are normally some approximations done concerning the geometry of the liquid jet and the intensity profile of the pump beam. Additional error is added when the probe beam geometry (normally under some angle to the pump beam) and its intensity profile comes in. What is more, the overlap between the pump and the probe beams may not be perfect. Still, this estimation helps to evaluate the value of the excited state fraction extracted from the experimental data. For a linear regime (the number of photons much smaller then the number of molecules) the formula

$$f = N_{ph0} \cdot (1 - 10^{-OD})/N_{mol} \tag{2}$$

can be used. $N_{ph0} \cdot (1 - 10^{-OD})$ stands for the number of photons absorbed by a solution with optical density OD. For high excited state fractions it is more reasonable to use the formula

$$f = N_{ph0} \cdot (1 - 10^{-OD\cdot(1-f)})/N_{mol} \tag{3}$$

which takes into account that excited molecules are removed from the system resulting in the concentration of the molecules being $c \cdot (1 - f)$ instead of c [3]. N_{ph0} is calculated dividing the the pulse energy by the energy of a single photon. The number of molecules in the illuminated volume is calculated as$N_{mol} = N_A \cdot c \cdot V$. The table S4 summarises the conditions for the three experiments.

Table S4: Excited state fraction for different pump-probe experiments in this work. N_{ph0} is the incident photon flux. $N_{ph} = N_{ph0} \cdot (1 - 10^{-OD})$

	N_{ph0}	N_{ph}	Illuminated dimensions [mm] (w×h×d)	N_{mol}	f_0	f(50 ps)	f fitted (50 ps)
TA	5.0e12	3.4e12	0.2×0.2×1.	3.8e13	0.089	0.036	
WAXS	4.0e13	3.8e13	0.15×0.12×0.3	4.1e13	0.63	0.25	0.086 (0.04–0.15)
XAS	5.3e12	5.0e12	(0.2-0.3) × (0.2-0.3) × 0.3	5.4e13	0.10-0.34	0.04-0.135	0.10

7 Estimation of the excited state fraction in the TR-WAXS experiment from TR-XES measurements

One approach to estimate the excited state fraction in a time-resolved experiment is to measure spectra of the references for the ground and the excited states and then to scale the area of the experimental transient spectrum with the area of the reference difference (the integral of absolute difference (IAD) method). This method was widely used to estimate the excited state fraction for Fe spin-crossover complexes out of X-ray emission spectra due to the dependence of Kα and Kβ emission lines shapes on the spin state of the metal [10]. In this work we applied a similar approach. The laser-off and laser-on spectra and their difference are shown in Fig.S11a. Copper (+1) and (+2) oxides were measured as reference samples. The difference between them was then compared to the experimental transient. The spectral shapes (and linewidths) of Cu_2O and $Cu_2(NSSN)_2$ were found to be different as shown in Fig.S11b. What is more, the exact energy shift between the Kα_1 of Cu(+1) and Cu(+2) was not known. Therefore, we could not get a well-defined value of the excited state fraction out of this experiment. However, from the literature it is known that the shift in energy between Kα_1 lines of the same element in different oxidation states is small: up to few tenths of eV [4, 11]. We assumed that the energy shift between Kα_1 of the ground and the excited state lies within 0–1 eV. Shifting the spectrum

of CuO relative to the spectrum of $Cu_2(NSSN)_2$ in this energy range, we calculated a set of possible transients. By scaling the maximal amplitude of the experimental transient to that of the calculated ones we obtained the excited state fraction of 0.04–0.15. (Bigger energy shift corresponds to smaller excited state fraction). These findings are in agreement with the value of f obtained from the analysis of TR-WAXS data (f=0.086). This experiment also shows that the chemical environment of copper matters for the shape of the Kα_1 emission line, and more suitable references should be chosen for reliable extraction of the excited state fraction.

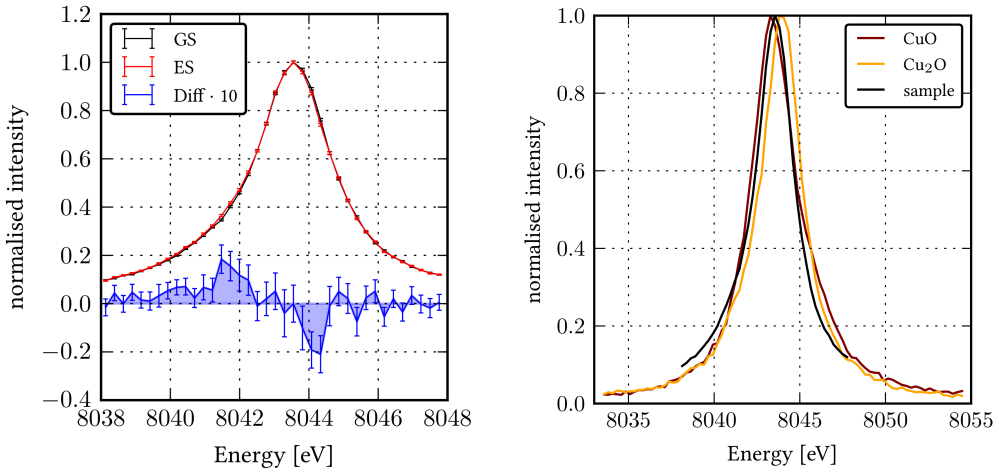

(a) Kα_1 spectra of the ground and photoexcited states and the difference between them.

(b) Spectra of copper oxides (references) and the sample.

Figure S11: TR-XES on $Cu_2(NSSN)_2$.

8 Lifetime of the excited state extracted from TR-XAS and TR-WAXS

The model for fitting of the excited state decay is based on the assumption that the pump instantaneously excites electrons from a ground state into an excited state, and the electrons in the excited state subsequently relax back to either ground state or an intermediate state **int** at a typical time τ after excitation. The progression of the decay suggests two well-separated lifetimes (one is infinitely long in the time scale of the experiment). Two models may be assumed: the two independent decay channels (parallel model) or subsequent decay of a fast-living state into the long-living state (serial model) (see Fig.S12). This modelling assumes that the contribution to the TR-XAS signal is the same for all excited or intermediate states. It essentially means that we see only excited states with Cu(II), because our signal comes from the edge shift to higher energies, and we assume that different excited states, as long as they are charge-transfer states, have the same edge positions.

Parallel model

This models describes the case of two excitation channels into excited states **1** and **2**. **1** decays to the ground state with the constant k_1, and **2** lives infinitely long in the time scale of the experiment. The populations of the excited states N_1, N_2 can be described as

$$\frac{dN_1}{dt} = -k_1 N_1 + c_1 P(t) \tag{4}$$

$$\frac{dN_2}{dt} = c_2 P(t) \tag{5}$$

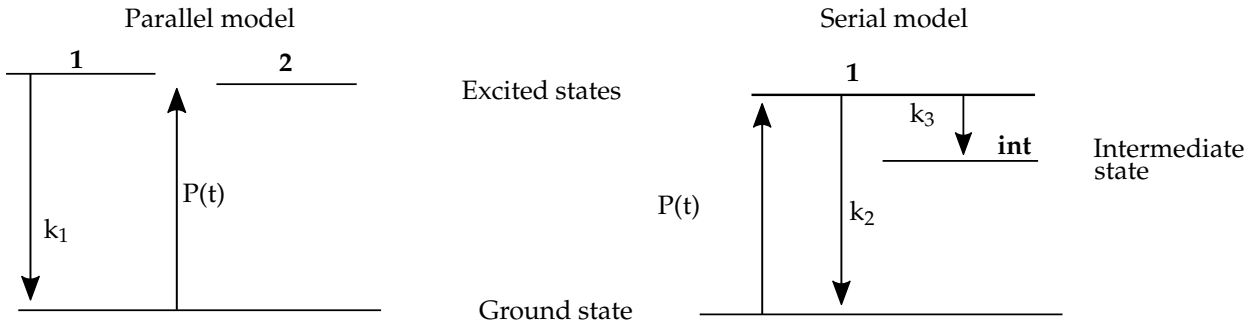

Figure S12: Schematic illustration of two excitation models.
Parallel model: the excitation populates two states **1** and **2**. State **1** decays with the rate constant k_1, state **2** does not decay.
Serial model: the excitation populates state **1**, which decays to the ground state with the rate constant k_2 and to the intermediate state **int** with the rate constant k_3. State **int** does not decay further.

where $P(t)$ is the pump pulse. For the Gaussian laser pulse with width σ_{pu} $P(t) = \frac{1}{\sqrt{2\pi}\sigma_{pu}} e^{-\frac{t^2}{2\sigma_{pu}^2}}$, and coefficients c_1 and c_2 include the pump intensity and excitation yield of the states **1** and **2**.

Solving this differential equation results in

$$N_1 = 1/2 \cdot c_1 \cdot e^{\sigma_{pu}^2 \cdot k_1^2/2} \cdot erfc(\frac{\sigma_{pu} \cdot k_1}{\sqrt{2}} - \frac{t}{\sqrt{2}\sigma_{pu}}) \cdot e^{-k_1 t} \tag{6}$$

$$N_2 = 1/2 \cdot c_1 \cdot erfc(-\frac{t}{\sqrt{2}\sigma_{pu}}) \tag{7}$$

$\sigma_{pu} \cdot k_1 \sim 10^{-4}$, therefore $e^{\sigma_{pu}^2 \cdot k_1^2/2} \approx 1$.

The next step would be convolution of the excited state population with the probe X-ray pulse. Since the probe pulse (70-100 ps) is much longer than the pump pulse (180 fs) we can neglect the width of the latter and approximate the excited state population with Heaviside step function $\theta(t)$:

$$N_1 = c_1 \theta(t) e^{-k_1 t} \tag{8}$$

$$N_2 = c_2 \theta(t) \tag{9}$$

The contribution of the both excited states to the signal will be:

$$N_1 + N_2 = c_2 \theta(t)(1 + \frac{c_1}{c_2} \cdot e^{-k_1 t}) \tag{10}$$

Serial model

This models describes the case when the excitation happens into excited state **1** which decays to the ground state with rate constant k_2 and to the intermediate state **int** with the constant k_3. The intermediate state does not decay further. The rate of depopulation of **1** is $k_1 = k_2 + k_3$.

The populations of the excited state N_1 and the intermediate state N_{int} can be described as

$$\frac{dN_1}{dt} = -(k_2 + k_3)N_1 + c_1 P(t) = -k_1 N_1 + c_1 P(t) \tag{11}$$

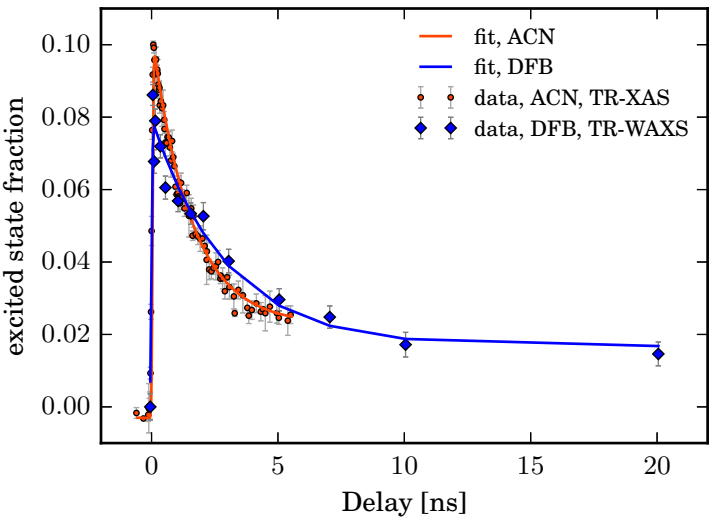

Figure S13: Time evolution of the excited state observed in TR-XAS and TR-WAXS experiments. Extracted excited state fraction is plotted as a function of time delay between the pump and the probe pulses. Red: transient XAS in ACN, $\tau = 1.53 \pm 0.04$ ns. Blue: transient WAXS in DFB, $\tau = 2.9 \pm 0.7$ ns. For fitting details see text.

$$\frac{dN_{int}}{dt} = k_2 N_1 \tag{12}$$

If we take the value for N_1 from eq. 8 and solve eq. 12 with it we obtain

$$N_{int} = c_1 \frac{k_2}{k_1} \theta(t)(1 - e^{-k_1 t}) \tag{13}$$

$$N_1 + N_{int} = c_1 \theta(t) \frac{k_2}{k_1} (1 + \frac{k_1 - k_2}{k_2} e^{-k_1 t}) \tag{14}$$

Comparison of the equations 10 and 14 shows that the models have essentially the same time dependence and cannot be distinguished without the prior knowledge on the base of fitting only. In both cases the faster decay is the rate of disappearance of the excited state **1**. Interpretation of amplitudes would be different for different models.

Convolution of the excited states populations (parallel model) with the probe signal $Pr = b_1 \cdot \frac{1}{\sqrt{2\pi}\sigma_{pr}} e^{-\frac{t^2}{2\sigma_{pr}^2}}$ results in the equation

$$dXAFS = 1/2 \cdot c_1 \cdot b_1 \cdot erfc(\frac{\sigma_{pr} \cdot k_1}{\sqrt{2}} - \frac{t}{\sqrt{2}\sigma_{pr}}) \cdot e^{-k_1 t} + 1/2 \cdot c_2 \cdot b_1 \cdot erfc(-\frac{t}{\sqrt{2}\sigma_{pr}}) \tag{15}$$

Eq. 15 was used to fit the lifetime data obtained in both TR-XAS and TR-WAXS experiments.

The kinetic traces of the decays measured in TR-XAS and TR-WAXS experiments with corresponding fits are shown in Fig.S13.

9 TR-WAXS: data analysis

The difference scattering signals were extracted using standard data reduction procedure described in details e.g. in ref. [6, 7]. Briefly, all the images were azimuthally integrated into 1D intensity curves $S(q,t)$ taking into account the linear polarisation of the incident X-ray beam, the scattering angle dependences of the detector efficiency and the space angle coverage of the flat detector. Additionally the signals were corrected for the sample absorption of X-rays, the non-sample related scattering background and the curves were normalised for fluctuations of the incoming X-ray flux. The individual $S(q,t)$ curves were converted to the electron units per solvent molecule taking into account the molar ratios of the solute over solvent and using the procedure of scaling the curves to the corresponding gas-phase scattering calculated by Debye equation in the high $q > 5$ Å^{-1} region (see e.g. [5]). The difference scattering signals were produced by subtracting the reference scattering $S(q, t = -3ns)$ of the unperturbed sample from curves with other delays $S(q,t)$ in the set to result in $\Delta S(q,t)$. After a Chauvenet's criterion based outliers rejection (typically less than 5% are outliers) the difference signals were averaged and the standard error of the mean curve was calculated to yield the error bars in the data.

Modelling of the difference scattering data for each pump-probe delay t was done with the following formula:

$$\Delta S(q,t)^{fit} = R \cdot \gamma(t) \cdot \Delta S(q)^{calc}_{solute} + \left(\left(\frac{\partial S(q)}{\partial T} \right)_{\rho} \cdot \Delta T(t) + \left(\frac{\partial S(q)}{\partial \rho} \right)_{T} \cdot \Delta \rho(t) \right)_{solvent} \tag{16}$$

In this equation the first term in the sum represents the contribution from the structural changes in the solute, the second accounts for changes in temperature and density of the solvent due to the deposited energy from relaxing solute molecules. The signal related to changes in solute-solvent inter-atomic distances due to excitation, also called the cage term, was not taken into account in the present analysis as it is only expected to considerably contribute at lower values of q below 1 Å^{-1} considering the expected characteristic dimensions of the solvation shell. The solute term $\Delta S(q)^{calc}_{solute}$ is the calculated difference signal between the excited and ground states of the molecule, $\gamma(t)$ is the excited state fraction and R is the molar ratio of solute to solvent molecules. The solute scattering signals for the ground and various excited structures were calculated according to the Debye equation as described e.g. in ref. [7] and then convoluted with the "pink" spectrum of the X-ray beam by computing a weighted sum of the scattering signals for 200 components equally spaced in energy over the entire spectrum. The derivatives $\left(\frac{\partial S(q)}{\partial T} \right)_{\rho}$ and $\left(\frac{\partial S(q)}{\partial \rho} \right)_{T}$ are the solvent-specific scattering responses to the ultrafast heating due to temperature increase and thermal expansion, thus the density decrease, of the solvent bulk [2]. The solvent-related differentials were obtained in a dye-mediated laser-induced solvent heating measurement [8] during the same experiment. No absolute calibration measurement was carried out for the differentials so the $\Delta T(t)$ and $\Delta \rho(t)$ represent the temperature and the density changes of the solvent only in arbitrary units which is nevertheless not a limitation for our analysis aiming at determining the solute structure in the excited state. For the following analysis the high frequency noise component in the solvent response differentials was reduced using Savitzky-Golay filter in order to limit the propagation of additional noise though the linear combination fit, as also proposed elsewhere [8, 2]. The filtering did not affect the overall shape of the difference curves only reducing the high frequency point-to-point fluctuations in the data. No filtering and no smoothing was applied for the sample solution data set.

The TR-WAXS data fitting using equation (16) was performed for one ground state structure and various structural models of the excited state as described in the main text. The goodness of the fit was evaluated by calculating the reduced χ^2_{red} estimator following the equation:

$$\chi^2_{red} = \frac{1}{N - p - 1} \sum_{q} \frac{(\Delta S(q,t)^{fit} - \Delta S(q,t)^{exp})^2}{\sigma^2}, \tag{17}$$

where N is the total number of q points, p - number of fitting parameters, σ^2 is the standard deviation for each data point, $\Delta S(q,t)^{exp}$ is the experimental difference scattering and $\Delta S(q,t)^{fit}$

is the theoretically predicted signal (16) for a given set of the non-structural fitting parameters ($\gamma(t)$, $\Delta T(t)$, $\Delta\rho(t)$) and a given excited state structure defined by the structural parameters, the torsion angle ant the configurational coordinate **Q** (see main text). The sum in (17) is calculated over all q points. To gain the statistical confidence for comparisons of structural models the χ^2_{red} values were averaged over all delays below 10 ns. A surface plot of χ^2_{red} values in the space of optimised structural parameters is shown in Fig.S14 while Fig.S15 represents different slices of χ^2_{red} surface.

For extracting the excited state population kinetics $\gamma(t)$, the minimisation of χ^2_{red} estimator over non-structural parameters was performed for the best selected structural model, i.e. using the refined values of the configurational coordinate and the torsion angle yielding the minimum of χ^2_{red} in Fig.S14. The resulting fits to the data are presented in Fig.S16. The maximum ES fraction at early delays reached approximately 0.09. The temperature and the density kinetics were extracted in arbitrary units for each delay, no density change component was observed for delays below 10 ns.

10 TR-WAXS: sensitivity of $\Delta S(q)^{calc}_{solute}$ to the structural parameters

Fig.S17 demonstrates the effect of changing the Cu-ligand bond lengths along the transformation path $S_0^{cr} \rightarrow T_1^{cr}$ (i.e. changing the configurational coordinate **Q**) and the Cu-S-S-Cu torsion angle on the shape of calculated solute difference scattering signal $\Delta S(q)^{calc}_{solute}$. As can be seen the structural changes in the first coordination shell along the transformation $S_0^{cr} \rightarrow T_1^{cr}$ lead to only minor variation in the $\Delta S(q)^{calc}_{solute}$ primarily affecting the signal amplitude rather then the phase of oscillations. Consequently the χ^2_{red} value is hardly sensitive to this parameter (see Fig.S14): small changes in the signal amplitude are compensated by adjusting value of the ES fraction $\gamma(t)$ in the fitting procedure. On the other hand the shape of $\Delta S(q)^{calc}_{solute}$ signal strongly depends on the torsion angle. In order to illustrate the cause of only one parameter mostly affecting the fit the distance changes between different pairs of atoms for both types of structural variations are plotted in figures S18 and S19. The changes are calculated relative to the starting structure ($\mathbf{Q} = 0.5$ and 52°).These plots show that variations of the configurational coordinate result in maximum changes of interatomic distances of 0.08 Å, whereas the torsion angle variations cause changes in distances between some atoms up to 1-2 Å. Therefore the shape of $\Delta S(q)^{calc}_{solute}$ exhibits much stronger dependence on the torsion angle variation within our range. The same changes of the interatomic distances are shown in Fig.S19 on the relative scale i.e. normalised by the value of the starting structure.

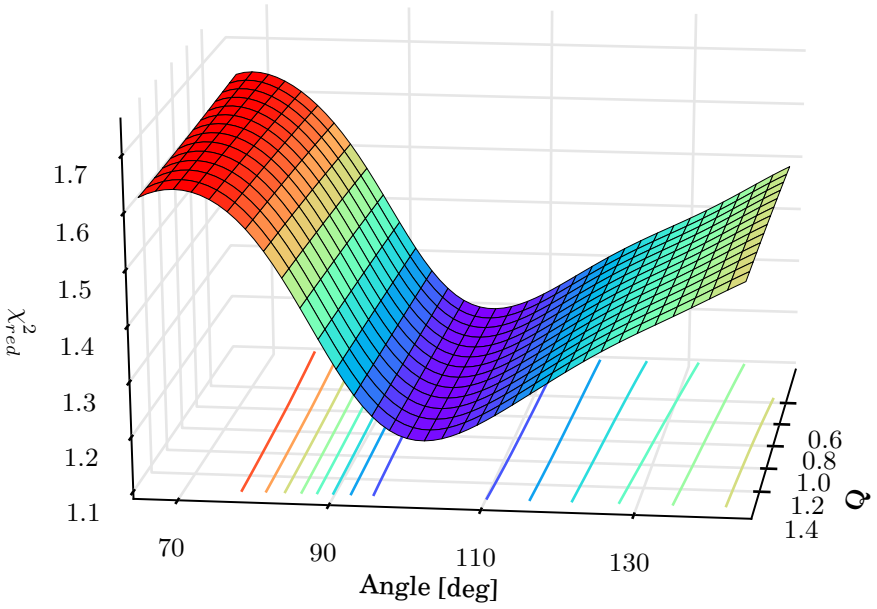

Figure S14: χ^2_{red} for fitting of TR-WAXS data as a function of the configurational coordinate **Q** (representing varying copper-ligand bond lengths, see main text) along the transformation path $S_0^{cr} \rightarrow T_1^{cr}$ and the torsion angle Cu-S-S-Cu (rotational angle between two parts of the molecule). For the values of torsion angle below 64° the fit was not successful as it returned negative value of the ES fraction.

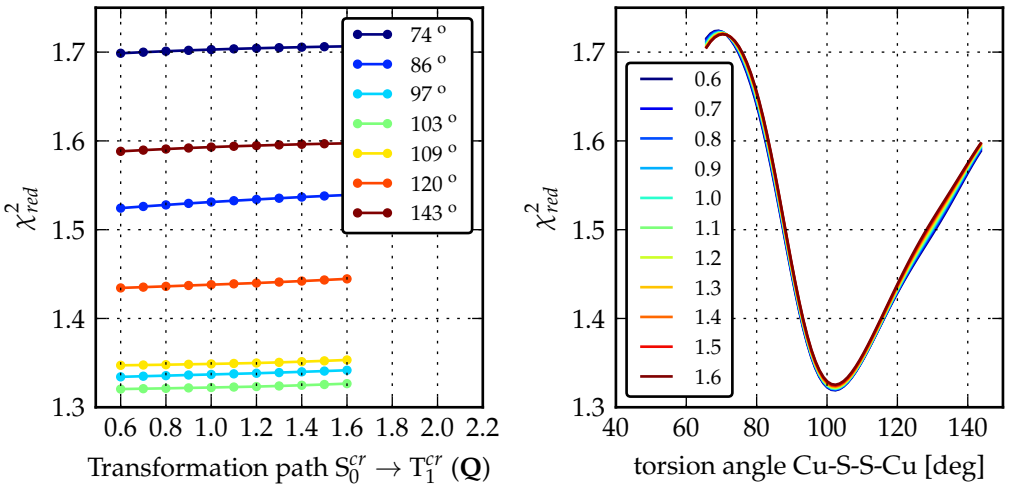

Figure S15: Slices of the χ^2_{red} surface shown in Fig.S14. a) χ^2_{red} as a function of configurational coordinate **Q** along the transformation path $S_0^{cr} \rightarrow T_1^{cr}$ for certain values of the Cu-S-S-Cu torsion angle; b) χ^2_{red} as a function of the torsion angle for the set of configurational coordinates.

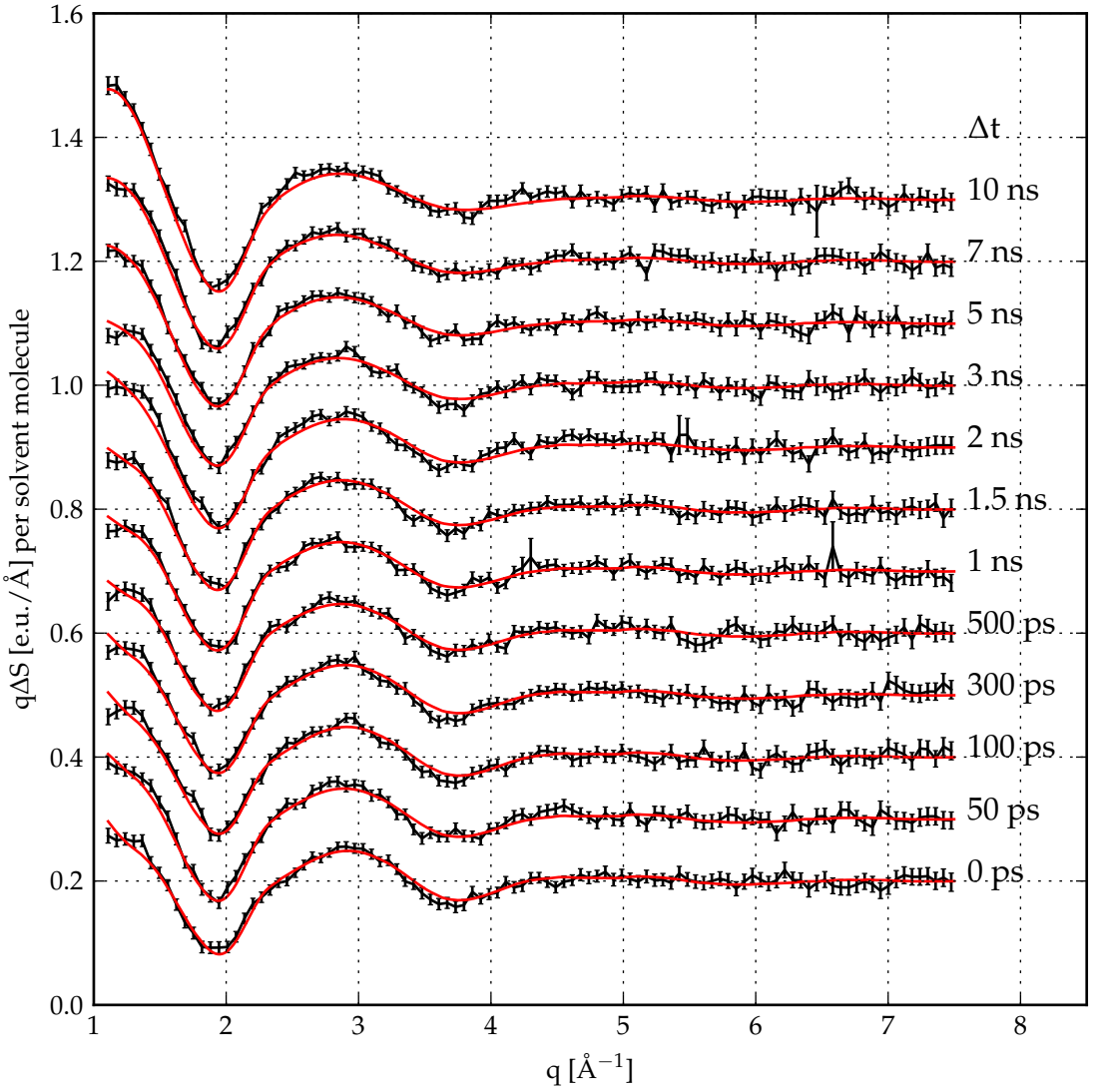

Figure S16: $q\Delta S(q)^{exp}$ (dots) and fitted $q\Delta S(q)^{fit}$ (red lines) for a set of pump-probe time delay in the TR-WAXS measurement.

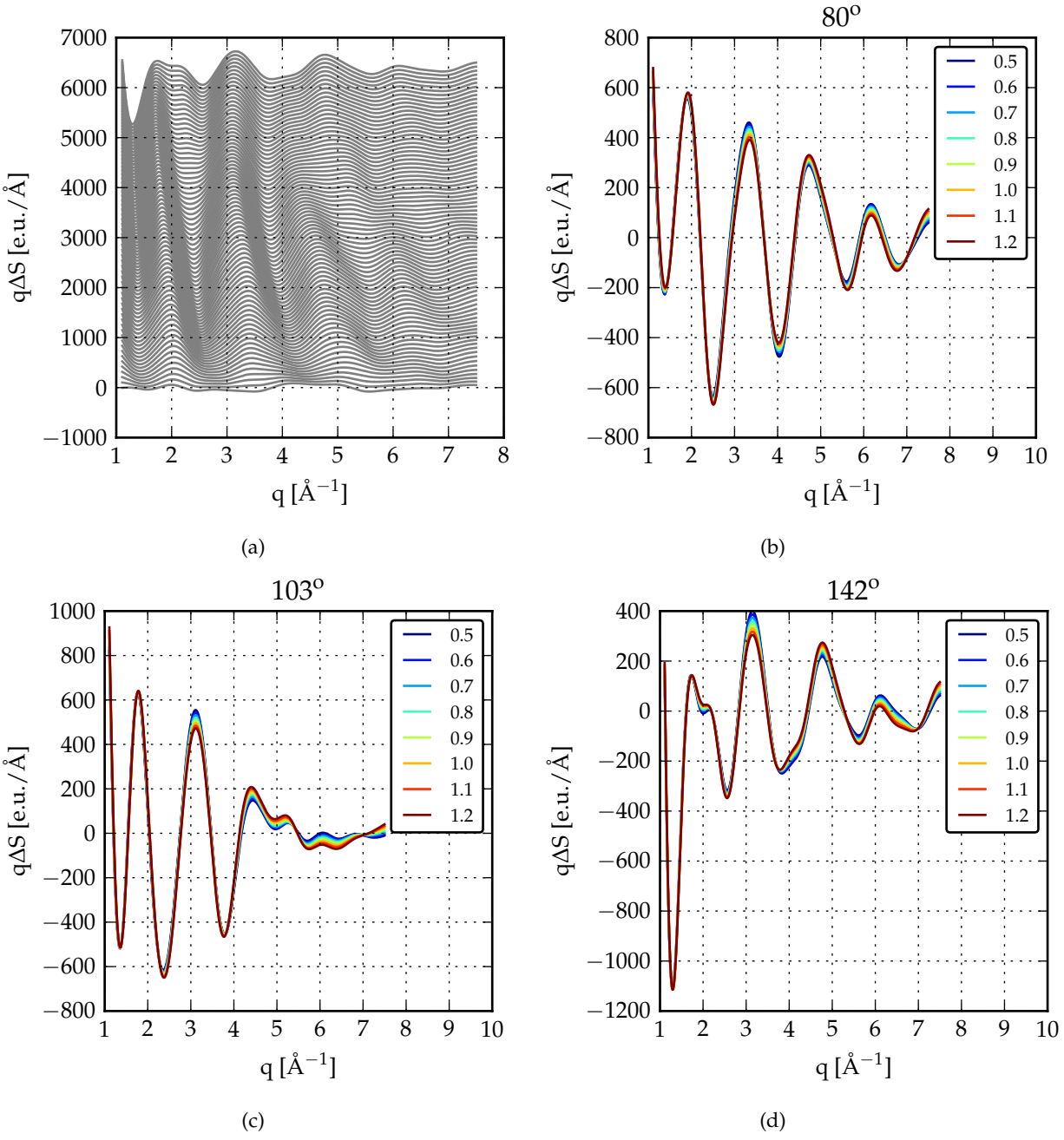

Figure S17: (a): Calculated solute difference signal $q\Delta S(q)^{calc}_{solute}$ for $\mathbf{Q} = 1.0$ with different torsion angles Cu-S-S-Cu. The angle linearly grows from the bottom to the top from 52° to 142°.(b), (c), (d): $q\Delta S(q)^{calc}_{solute}$ for fixed torsion angles Cu-S-S-Cu and various values of $\mathbf{Q}$.

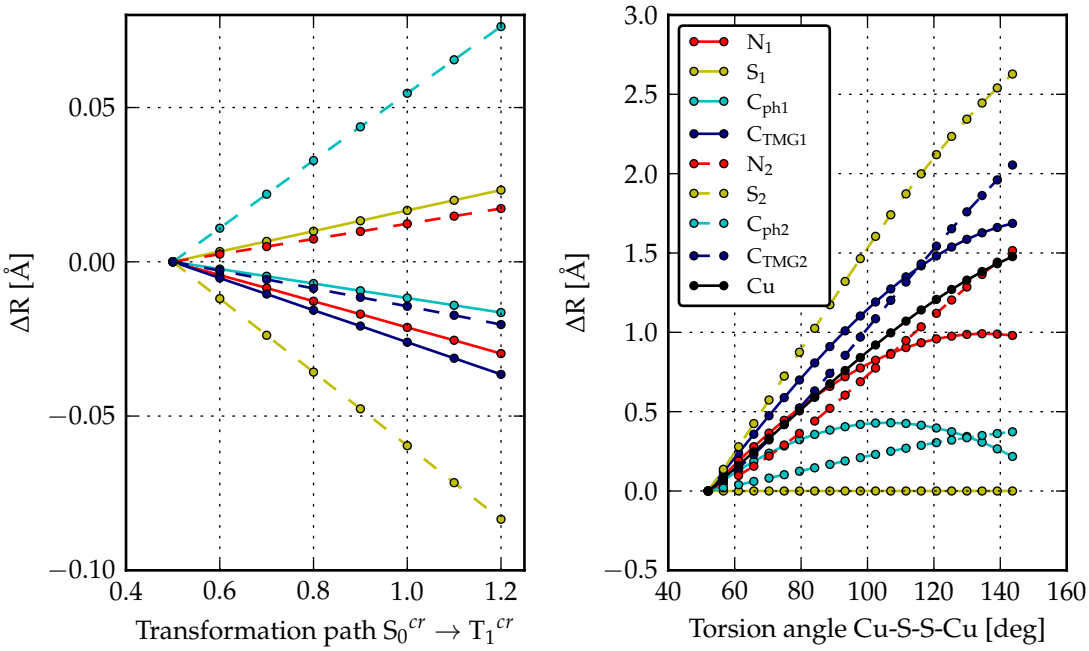

Figure S18: Margins of distance changes between different pairs of atoms during the structural refinement. For details see text. Left: distance changes from Cu_1 to atoms of its ligand upon coordination sphere refinement: coordinating nitrogen and sulfur (N_1,N_2,S_1,S_2), a carbon of phenyl group (C_{ph1}, C_{ph2}), a carbon of TMG group (C_{TMG1}, C_{TMG2}). Indices 1 and 2 denote two different ligands. Right: distance change from Cu_2 to the atoms shown on the left figure upon change of the torsion angle Cu-S-S-Cu. Additionally Cu_1-Cu_2 distance change is shown. From all distances the starting value is subtracted in order to bring them to the same scale.

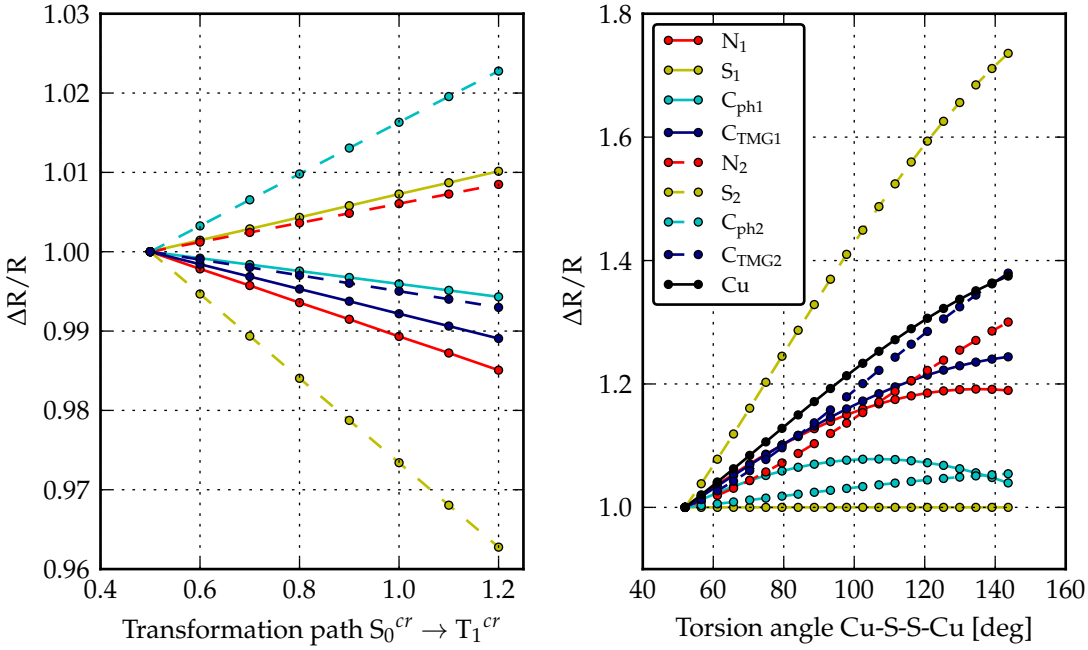

Figure S19: The same as in Fig.S18 shown in relative units: distance changes are normalised by division by the starting value at.

11 Technical description of the setup for transient absorption in UV-Vis

The TA setup is based on an amplified Ti:sapphire laser (Astrella, Coherent). The oscillator (Vitara, Coherent) is pumped by a 5 W CW semiconductor laser (Verdi, Coherent) and delivered ultrashort pulses (<35 fs) with energy of 25 nJ at repetition rate of 80 MHz and wavelengths of 800 nm. These pulses are amplified in a regenerative amplifier (Astrella, Coherent) pumped by a 38 W, 1 kHz intracavity frequency-doubled Nd:YLF laser (Revolution, Coherent). The final output delivers pulses characterised by 33 fs duration at 800 nm with energy 6.5 mJ/pulse at 1 kHz repetition rate. The majority of the output energy of the fundamental beam is frequency doubled by the second harmonic generation (SHG) in a 0.3 mm thick barium betaborate (BBO) crystal to generate pump pulses at 400 nm wavelength. The pump pulses at the sample position had total energy about 2.5 μJ and a diameter about 0.4 mm. The remaining energy (a few μJ) of the fundamental beam is used to generate a 340 –750 nm white light supercontinuum by focusing in a 2 mm thick CaF_2 rotating plate, which serves as a probe. The pump-probe polarisation configuration is set at the magic angle (54.7′), and the probe pulse is delayed in time relative to the pump pulse using an optical delay line (M-IMS1000LM Linear Stage, Newport). The probe and pump beams are focused and overlapped on the quartz sample cell with 1 mm path length. The transmitted light of the probe is focused onto the entrance slit of a prism spectrograph and recorded by a CCD camera (HA S7030-1006, 1024 $\times$ 64 px, Hamamatsu). The shot to shot readout of the CCD camera is synchronised with the laser amplifier by a electronic system (Entwicklungsbuero Stresing) and pump on/off cycles are obtained by the chopper placed in the pump beam working at 500 Hz and synchronised with the laser amplifier. All the pump off and pump on recorded spectra are transferred to the computer via PCI interface and the transient absorption spectra are computed.

12 Comparative kinetic behaviour of $Cu_2(NSSN)_2(PF_6)_2$ and $Cu_2(NSSN)_2(OTf)_2$ in ACN, DCM and DFB extracted from the TA in UV-Vis measurements

Table S5: Time constants obtained by global fit analysis of transient absorption spectra for $Cu_2(NSSN)_2$ with PF_6 and OTf counter ions in different solvents.

Solvent	Counter-anion	τ_1 / ps	τ_2 / ps
DFB	PF_6	0.65 ± 0.03	10.6 ± 1.8
	OTf	0.70 ± 0.09	12.5 ± 3.1
ACN	PF_6	0.53 ± 0.06	7.9 ± 1.0
	OTf	0.61 ± 0.05	11.1 ± 1.8
DCM	PF_6	0.47 ± 0.11	7.4 ± 2.1
	OTf	0.94 ± 0.21	12.7 ± 5.0

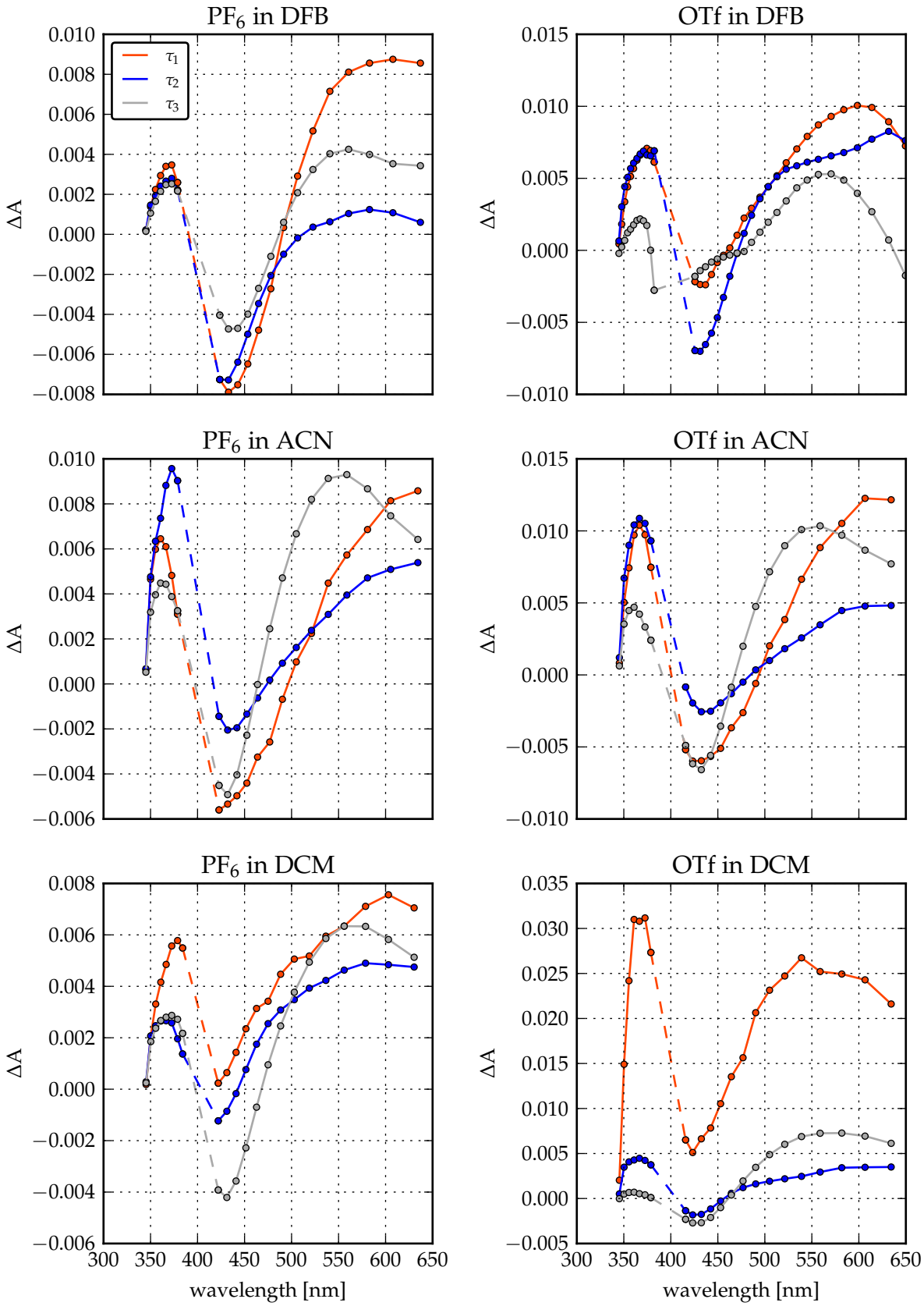

Figure S20: Decay associated spectra from transient absorption of $Cu_2(NSSN)_2(PF_6)_2$ and $Cu_2(NSSN)_2(OTf)_2$ in ACN, DCM and DFB obtained by global fit analysis with multi-exponential functions. Time constants are given in Table S5.

References

[1] N. Binsted. *EXCURV98: CCLRC Daresbury Laboratory Computer Program*. CCLRC Daresbury Laboratory, Warrington, UK. 1998.

[2] M. Cammarata et al. "Impulsive solvent heating probed by picosecond x-ray diffraction". In: *The Journal of Chemical Physics* 124.12 (2006), p. 124504. eprint: `http://dx.doi.org/10.1063/1.2176617`.

[3] Lin X Chen et al. "MLCT State Structure and Dynamics of a Copper (I) Diimine Complex Characterized by Pump - Probe X-ray and Laser Spectroscopies and DFT Calculations". In: *Journal of American Chemical Society* 125 (2003), pp. 7022–7034.

[4] Pieter Glatzel. "X-Ray Fluorescence Emission Following K Capture and 1s Photoionization of Mn and Fe in Various Chemical Environments". 2001.

[5] Greg Hura et al. "A high-quality x-ray scattering experiment on liquid water at ambient conditions". In: *The Journal of Chemical Physics* 113.20 (2000), pp. 9140–9148. eprint: `http://dx.doi.org/10.1063/1.1319614`.

[6] H. Ihee. "Ultrafast X-ray Diffraction of Transient Molecular Structures in Solution". In: *Science* 309.5738 (Aug. 2005), pp. 1223–1227.

[7] Hyotcherl Ihee et al. "Ultrafast X-ray scattering: structural dynamics from diatomic to protein molecules". In: *International Reviews in Physical Chemistry* 29 (2010), pp. 453–520.

[8] Kasper Skov Kjær et al. "Introducing a standard method for experimental determination of the solvent response in laser pump, X-ray probe time-resolved wide-angle X-ray scattering experiments on systems in solution." In: *Physical chemistry chemical physics : PCCP* 15 (2013), pp. 15003–16.

[9] B. Ravel et al. "ATHENA, ARTEMIS, HEPHAESTUS: Data analysis for X-ray absorption spectroscopy using IFEFFIT". In: *Journal of Synchrotron Radiation* 12.4 (2005), pp. 537–541.

[10] György Vankó et al. "Detailed Characterization of a Nanosecond-Lived Excited State: X - ray and Theoretical Investigation of the Quintet State in Photoexcited $[Fe(terpy)_2]^{2+}$". In: *The journal of physical chemistry C* 119 (2015), pp. 5888–5902.

[11] György Vankó et al. "Probing the 3d Spin Momentum with X-ray Emission Spectroscopy : The Case of Molecular-Spin Transitions". In: *Journal of Physical Chemistry B* 110 (2006), pp. 11647–11653.